32 KSME Journal, Vol.4, No.1, pp. 32~39, 1990.

PREDICTION OF THE PENETRATION DEPTH IN LASER BEAM WELDING

Jae-Do Kim*

(Received September 7, 1989)

Three dimensional solution for the heat flow in laser beam welding with a constant moving Gaussian heat source has been analyzed. The temperature rise and cooling rate are related to the beam spot size, travel speed and laser power. As an application of this model, the theoretical predictions were compared to the experimental data in which laser conditions were arranged for carbon and AISI 316 steels as bead-on-plate welds, using a continuous wave 3kW CO_2 laser with the various travel speed, beam sport size and laser power. Experimental data show a good agreement with the theoretical predictions. This analytical model can be used to determine the maximum possible penetration depth, fusion boundary, and thermal history for given sources of laser beam welding conditions.

Key Words : Laser Beam Welding, Penetration Depth, Bead Width, Cooling Rate, CO_2 Laser, Gaussian Beam

1. INTRODUCTION

High power CO_2 laser beams are used in a wide variety of materials processing applications such as cutting, welding, and surface treatment. High power laser beam welding is a high energy density, low heat input process that offers the oppertunity to join matals. The principal variables of laser beam welding are the physical properties of material, the laser beam power, the beam spot size and the travle speed.

In metal welding, the most important metallurgical data are : (1) the thermal cycle in weld zone and heat-affected zone, which determines the extend of any phase change, (2) the peak temperature distribution and (3) the cooling rate which would affect the formation of metastable structures such as martensite. Without a mathematical model the values of these parameters are very difficult to obtain.

The effects of materials processing with a laser depend upon many variables, some of which are not easy to control or monitor. Therefore, it is very useful to theoretically predict the experimental trends to establish the understanding of laser beam welding process. In penetration welding with a laser it is very important to be able to predict the maximum possible penetration depth for given sources and to calculate the effects of varying any parameter.

A number of solutions to the heat conduction equations with different source terms, boundary conditions, and initial conditions were methodically given by Carslaw and Jaeger (1959). To allow for the keyhole effect, Swift-hook and Gick(1973) developed a two dimensional analytical model based on line heat source moving across the subtrate, which is unsuitable to calculate the penetration depth. The themal analysis reported by Cline and Anthony(1977) seems to be the realistic analytical model. However, their solution assumes that all the laser energy is absorbed at the material surface, which is appropriate only semiconductors. A three dimensional quasi steady state heat transfer model with a moving Gaussian heat source was developed by Mazumder and Steen (1980) using a finite difference numerical technique, which accounts for keyholing. The reflectivity was assumed to be zero at any surface position and the model is very sensitive on the input data. Davies et al. (1985) developed the modeling of the fluid flow in laser beam welding. They treated the motion of the molten pool and assumed that the cross sections of keyhole and molten pool are circular for analytical model, Unfortunately, the penetration depth is not able to be calculated.

This approach is considered for the reflectivity to obtain accurate temperature profile by a moving Gaussian laser beam. The calculation is extended to determine the penetration depth, bead width and cooling rate which is important in predicting metallurgical structures. This model can also be applied for laser spot welding, which takes account of the pulse duration.

As an application of this model, the theoretical results were compared to the experimental data in which laser welding conditions were arranged for the carbon and AISI 316 stainless steels. The agreement between the theoretical predictions and the experimental results on penetration depth and bead width has been found to be excellent.

2. THE PHYSICAL MODELING

A coordinate system is fixed in the material as shown in Fig. 1. The laser beam is parallel to the z-axis and moves in the x-direction at a constant velocity, v. The intensity distribution of the laser beam is Gaussian along the axes when the laser radius is defined as the radial distance at which the power density falls to $1/e^2$ of the central value. A Gaussian beam radius may be defined as the radius where the power has dropped to $1/e^2$ or 1/e of the central value. The beam

*Department of Mechanical Engineering, Inha University, Inchon 402~751, Korea.

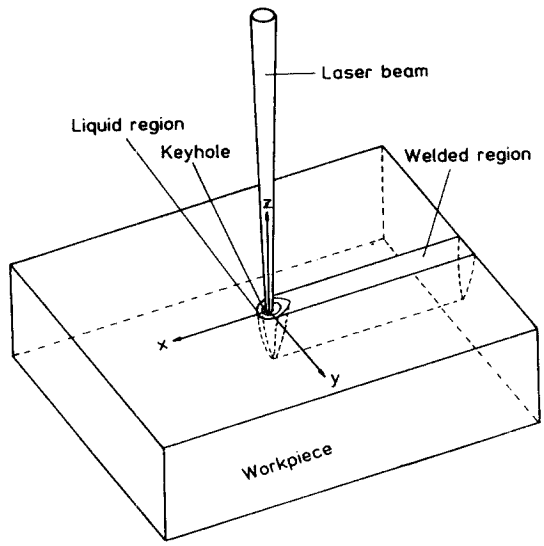

Fig. 1 Schematic illustration of laser bean melting by a Gaussian laser beam moving in the x-direction at a constant velocity

radius defined on the basis of $1/e^2$ contains more than 86% of the total power whereas the power contained for $1/e$ beam definition is slightly over 60% (Hull et al., 1985).

In the material, the laser beam is exponentially attenuated with an absorption coefficient α. In general, the laser beam is turned on at time $-t_1$ and turned off t_2. Hest loss from the surface is assumed to be negligible compared to conduction into the material. The thermal conductivity(K), density (ρ), and specific heat (C) are assumed to be independent of temperature. The material is assumed to be much thicker than penetration depth.

The time dependent heat diffusion equation is

$$\nabla^2 T=\frac{1}{r}\frac{\partial T}{\partial t}-\frac{G}{K} \tag{1}$$

where k is the thermal diffusivity and G is the heat source function which is defined as follows(Kim et al., 1988).

$$G=\frac{2\alpha(1-R)P}{\pi\delta^2}\cdot\exp[-2(x-vt)^2/\delta^2-2y^2/\delta^2-\alpha z] \tag{2}$$

in which P is the incident laser power, R is the reflectivity, and δ is the radius of beam spot defined as the radial distance at which the power density falls to $1/e^2$ of the central value. The solution can be expressed in terms of normalized variables where $x=\sqrt{2}x/\delta$, $\xi=\sqrt{2}y/\delta$, $\zeta=\alpha z$, $\tau=8kt/\delta^2$, $\nu=v\delta/4\sqrt{2}k$, $\gamma=\alpha\delta/2\sqrt{2}$, and θ is a normalized temperature rise. Given that,

$$T(x, y, z, t)=[P(1-R)/(2\sqrt{2\pi}K\delta)]\cdot\Theta(\chi, \xi, \zeta, \tau, \nu, \gamma) \tag{3}$$

$$\begin{aligned}&\Theta(\chi, \xi, \zeta, \tau, \nu, \gamma)\\&=(\gamma/2\sqrt{\pi}\int_{\tau_0}^{\tau+\tau_1}[\exp(\gamma^2\tau')/(\tau'+1)]\\&\cdot\exp[-\{(\chi-\nu(\tau-\tau'))^2+\xi^2\}/(\tau'+1)]\\&\cdot[\exp(\zeta)\cdot\mathrm{erfc}(\gamma\sqrt{\tau'}+\zeta/2\gamma\sqrt{\tau'})\\&+\exp(-\zeta)\cdot\mathrm{erfc}(\gamma\sqrt{\tau'}-\zeta/2\gamma\sqrt{\tau'})]d\tau'\end{aligned} \tag{4}$$

where

$$\begin{aligned}\tau_0&=0,\ -\tau_1<\tau<\tau_2\\&=\tau-\tau_2,\ \tau>\tau_2\end{aligned}$$

It can be found that the normalized temperature rise depends on two normalized parameters : a normalized velocity, ν, which is the ratio of the scanning velocity of the laser beam to the ratio of heat diffusion in the material, and a geometrical factor, γ, which is the ratio of the beam spot radius to the absorption depth.

For a continuous scanning beam, the start and stop times t_1 and t_2 are infinite. The solution can be considered to be several specific situations. One is interested in the maximum temperature rise in the material, which occurs at the surface $z=0$ in the center of the scan at $x=y=0$. The normalized temperature rise at this point is given by $\theta(0, 0, 0, \tau, \nu, \gamma)$. This is more detailed in section 3.2.

If the laser beam is stationary, the heat equation with $\nu=0$ would become the time-independent Poisson's equation. This is a steady-state solution since the rate at which energy is delivered by the beam is balanced by the rate of heat conduction into material. The normalized temperature rise depends only on the geometricl factor r. The largert temperature rise occurs when γ is infinite. When the scan speed is much faster than the rate of thermal diffusion, *i.e.*$\nu\to\infty$, the temperature distribution is just the Gaussian profile of the optical laser beam(Kim et al., 1988).

The cooling rate is related to the thermal gradient in the direction of the beam motion. The gradient is found by differentiation of Eq.(3) to yield an integral expression as follows.

$$\frac{\partial T}{\partial t}=[Pv(1-R)/\sqrt{\pi}K\delta^2]\cdot\Psi(\chi, \xi, \zeta, \tau, \nu, \gamma) \tag{5}$$

$$\begin{aligned}&\Psi(\chi, \xi, \zeta, \tau, \nu, \gamma)\\&=(\gamma/\sqrt{\pi})\int_{\tau_0}^{\tau+\tau_1}[\chi-\nu(\tau-\tau')]/(\tau'+1)\\&\cdot[\exp(\gamma^2\tau')/(\tau'+1)]\\&\cdot\exp[-\{(\chi-\nu(\tau-\tau'))^2+\xi^2\}/(\tau'+1)]\\&\cdot\exp[-\{(\chi-\nu(\tau-\tau'))^2+\xi^2\}/(\tau'+1)]\\&\cdot[\exp(\zeta)\cdot\mathrm{erfc}(\gamma\sqrt{\tau'}+\zeta/2\gamma\sqrt{\tau'})\\&+\exp(-\zeta)\cdot\mathrm{erfc}(\gamma\sqrt{\tau'}-\zeta/2\gamma\sqrt{\tau'})]d\tau'\end{aligned} \tag{6}$$

in which Ψ is a normalized cooling rate.

3. EVALUATION OF TEMPERATURE DISTRIBUTION

3.1 Optical Properties of Materials

The reflectivity of materials varies with the wavelength of the laser beam, the surface condition and the temperature.

Table 1 The thermophysical properties of the tested materials.

	Carbon steel	AISI 316
Thermal conductivity (W/cm℃)	0.24	0.24
Thermal diffusivity (cm²/sec)	0.055	0.045
Absorption coefficient(cm^{-1})	6.0	6.0
Reflectivity	0.3	0.3
Vaporizing point(℃)	2870	2870
Melting point(℃)	1530	1500

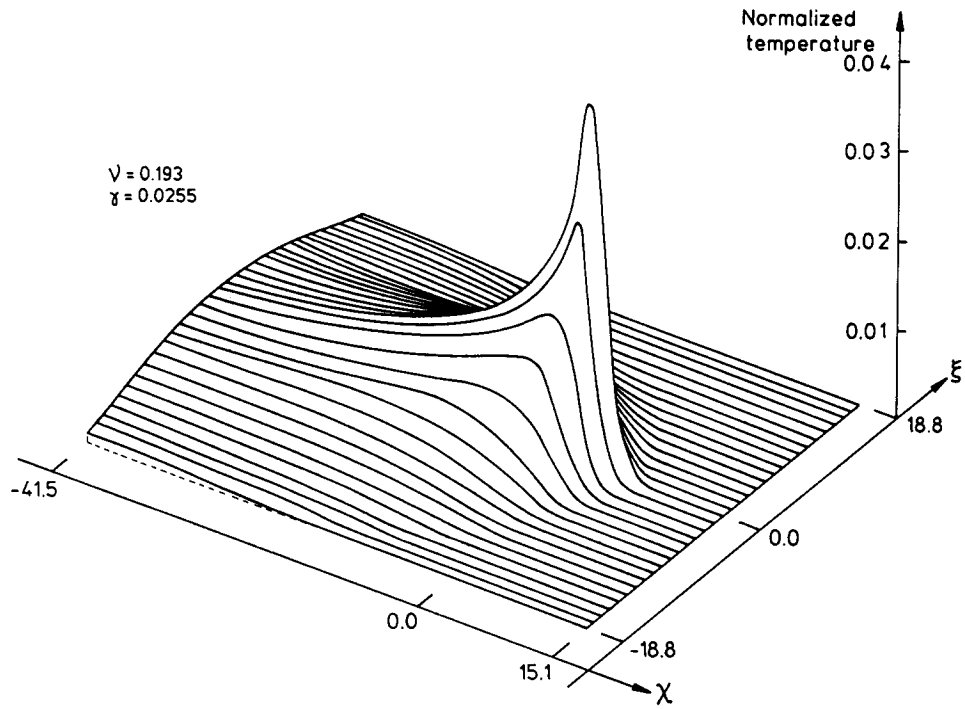

Fig. 2 Typical normalized surface temperature profile of carbon steel with a laser power of 2.0 kW, a travel speed of 3 m/min, and a beam spot radius of 120μm

The reflectivity of all metals is high at long infrared wavelengths. The incident radiation is partly reflected and is partly absorbed. Most of metals at room temperature are highly reflective at the wavelength of 10.6μm. When the surface temperature reaches the melting point, the absorption of the beam energy in steel rises dramatically (Walker, 1984). A part of the incident radiant power which falls on a keyhole is considered to pass into the keyhole losing some power by absorption and reflection within the keyhole.

The reflectivity of the carbon and stainless steels is chosen properly as 0.3 during the CO_2 laser welding in this calculation. Breinan and Banas (1975) noted that incident beam energy between 54% and 94% was absorbed by the workpiece. Adams (1973) has shown that typically 70% of beam power was absorbed by the steels.

The absorption coefficient α of a material gives the power density attenuation per unit length. According to some authors (Maher et al., 1974 ; keefer et al., 1975), the absorption coefficient due to free carrier increases as the wavelength of the incident beam increases. Unfortunately, data of the absorption coefficient in steel are lacking. Mazumder and Steen (1980) used 8cm^{-1} as α value for mild steel, Klemens (1976) 6cm^{-1} and Schuöcker (1985) also 6cm^{-1}. This study uses 6cm^{-1} as the value of the absorption coefficient for the carbon and stainless steels. The average values of the thermophysical properties of the tested materials(Touloukian, 1975) have been used for calculation as shown in Table 1.

3.2 Normalized Temperature Rise

A typical three-dimensional normalized temperature profile on the surface material is shown in Fig. 2. The normalized temperature rise across the laser beam at $t=0$ at any point of the material is given from Eq. (4). These are illustrated in Figs. 3 and 4. Figure 3 shows the normalized temperature rise on the material surface for different normalized velocities. As the normalized velocity increases, the maximum temperature decreases and shifts behind the center of the moving laser eam, since the total energy delivered to any point on the material becomes smaller as the dwell time of the beam decreases. When the normalized velocity is much slower and approaches to 0, the maximum temperature does not increase indefinitely and is limited by heat loss through conduction.

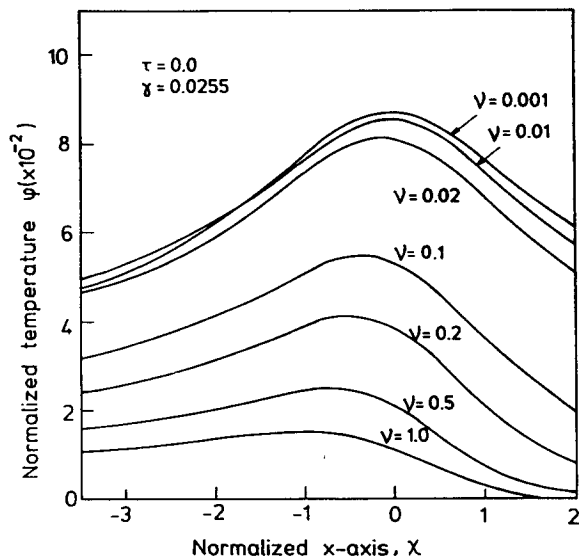

Fig. 3 Normalized temperature rise (Θ) on the surface as a function of χ for different normalized velocities (ν) ranging from 0.001 to 1.0 in carbon steel

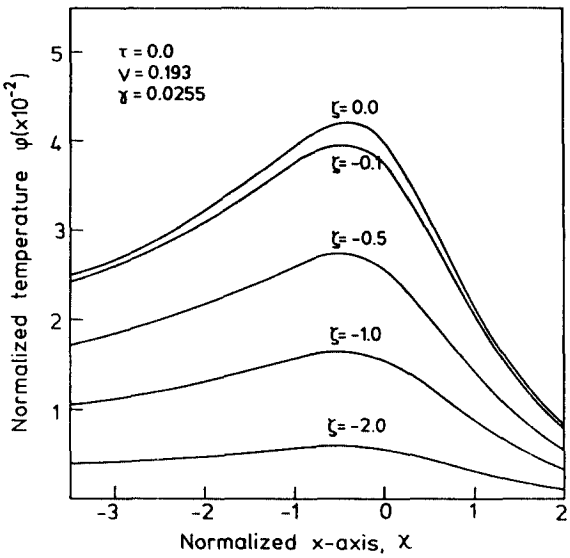

Fig. 4 Normalized temperature rise (Θ) as a function of χ for a normalized velocity (ν) at different values of the normalized depth (ζ)ranging from 0.0 to −2.0 in carbon steel

Although the center of the beam passes the origin ($x=y=0$) at $t=0$, the maximum temperature rise generally occurs at some time $t>0$. For $t>0$, the beam is still delivering energy from its Gaussian tail, and at the some time heat is diffusing away from the origin both laterally and into the bulk of the material. Generally, the temperature diminishes with the depth z and with the distance y perpendicular to the laser beam direction.

3.3 Cooling Rate

Figure 5 shows the normalized cooling rate at different depth. The maximum cooling rate decreases with increasing material depth. The maximum cooling rate is typically calculated to be 7.2×10^5 ℃/sec with a laser power of 2 kW and a travel speed of 3m/min. The lower the applied energy per unit length is, the higher is the cooling rate. The cooling rate from 800℃ to 500℃ ($\Delta t_{8/5}$) is most important in laser materials processing because in most steels it represents the A_3 transformation. In molten zone generated at a laser power of 2kW and a travel speed of 3m/min, the $\Delta t_{8/5}$ is calculated to be greater than 10^3 ℃/sec and passage is very short in duration.

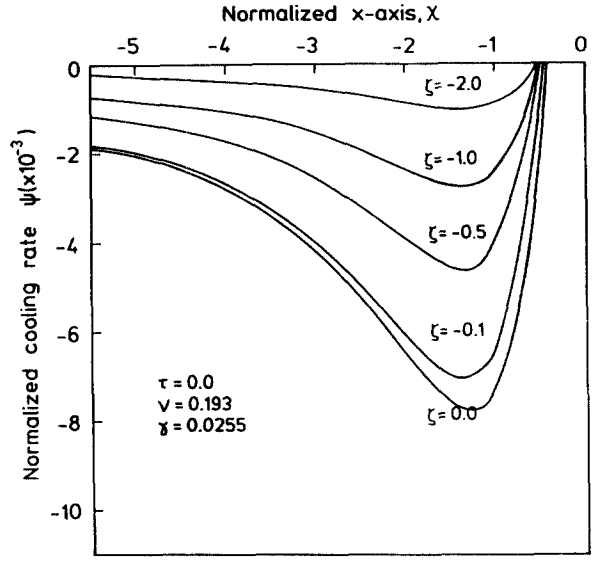

Fig. 5 Normalized cooling rate distribution for a normalized velocity (ν) at different values of the normalized depth ranging from 0.0 to −2.0 in carbon steel

4. EXPERIMENTS

4.1 Materials

In order to test the validity of the assumed model, the 6mm thick carbon steel and 6 mm thick AISI 316 stainless steel were melted as bead-on plate. The specimens of carbon steel consisted of rectangular sheets, 500mm long and 100mm wide. Those of AISI 316 steel were 200mm long and 100mm wide. The chemical compositions of the tested steels are shown in Table 2.

Table 2 The chemical compositions of materials (wt%)

	C	Mn	Si	P	S	Cr	Ni	Mo	Nb
Carbon steel	0.127	0.71	0.003	0.001	0.006				
AISI 316	0.054	1.65	0.49	0.02	0.012	17.1	12.5	2.23	0.005

4.2 Description of Laser System

The experimental data were generated by using a continuous wave 3kW CO_2 laser which was manufactured by CBL Optronics. The laser is of a fast axial flow type and is linked to a working station including a NC table. The laser beam is reflected down and focused by a ZnSe lens with a focal length of 127mm. The incident beam power is reduced about 20% of output beam power because of the beam divergence and the absorption of the optic system during delivering from the laser system to the working station.

4.3 Description of Laser Beam Welding

The laser power ranged from 1.0 to 2.5kW and the travel speeds were 0.5, 1.0, 1.5, 2.1, 3.0, 4.2, and 5.1m/min at each power level. The focal position was 1.0 and 2.0mm below the surface of material in carbon steel and was 1.0mm in stainless steel. The beam radius focused 1.0mm below the surface of material with Gaussian beam mode was approximately calculated to be 120μm. In case of focusing 2.0mm below, that was calculated to be 150μm. The specimens were degreased with acetone just before laser melting. Argon was used as a shielding gas with a flow rate of 20 1/min. Three trials at each combination of parameters were performed to establish the statistical variability.

To measure the penetration depth and the bead width, transverse sections were taken 50mm from the end of each melt. The mounted specimens were etched using 2% Nital for 20sec in carbon steel and using Glyceregia solution in AISI 316 steel.

5. RESULTS AND DISCUSSION

From the weldng point of view, the main interest is the

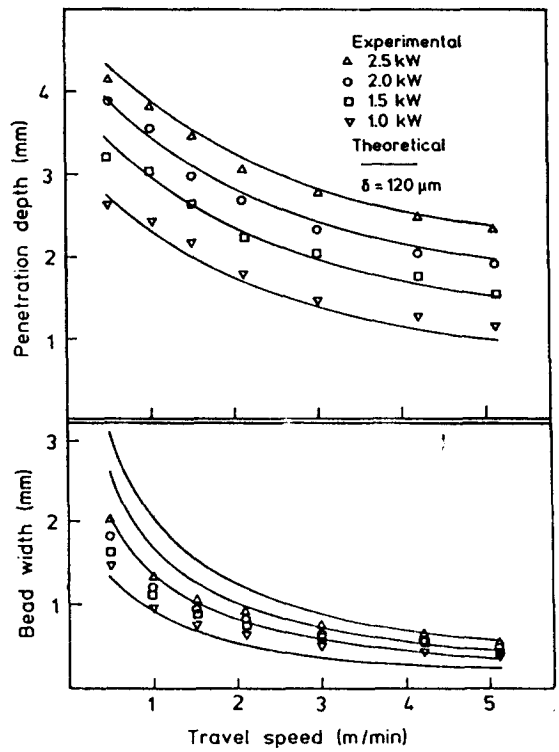

Fig. 6 Comparison of the experimental results with the theoretical model on penetration depth and bead width as a function of travel speed at various laser powers when a focal position is 1.0mm below the material surface in 6mm thick carbon steel

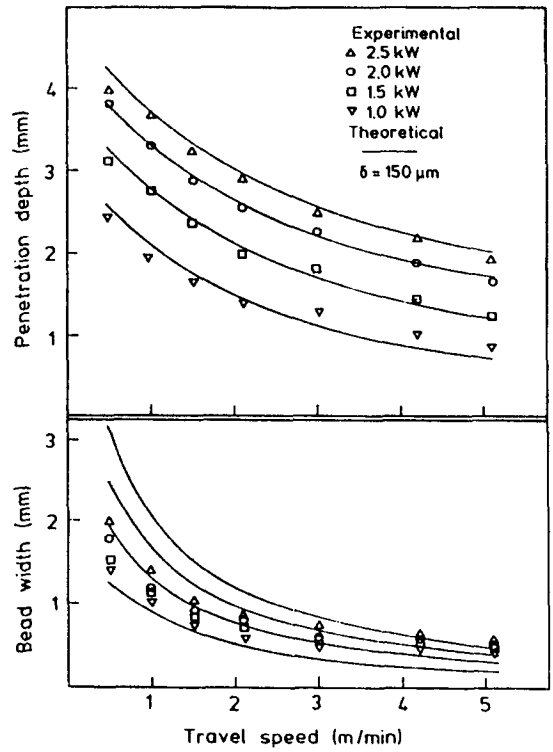

Fig. 7 Comparison of the experimental results with the theoretical model on penetration depth and bead width as a function of travel speed at various laser powers when a focal position is 2.0mm below the material surface in 6mm thick carbon steel

prediction of penetration depth, bead width and heat-affected zone in a given material corresponding to the laser beam spot size, laser power and travel speed. Figure 6 shows the comparison between the calculated and expdeimentally obtained penetration depths and bead widths with laser power varying between 1.0 and 2.5kW and travel speed between 0.5 to 5.1 m/min in carbon steel. Figure 7 shows the comparison with the other focal position of 2.0mm below the surface of material. The comparison in AISI 316 steel is shown in Fig. 8.

As shown, the predicted and exprimentally obtained penetration depths are in a very good agreement with each other for this range of laser power and travel speed. But the calculated and experimentally obtained bead widths slightly differ with each other. At high travel speed the calculated bead widths have a tendency to be narrower than the experimetal ones whereas at low travel speeds the calculated ones are somewhat wider than the experimental results.

The effect of focus position by focusing to 2.0mm below the surface of the workpiece is significant on penetration depth. It can be seen that the penetration depth is lower than that of the former case, obtaining by focusing to 1.0mm below the surface of the workpiece.

In laser welds of AISI 316 steel, the experimentally obtained bead width is wider than that of carbon steel welds. At low speed the plasma produced during the laser beam welding acts like a secondary heat source above the keyhole, resulting in a big diameter heat source, and causing a wide weld bead. Therefore, the experimentally obtained bead width is wide and the shape obivously increases distortion

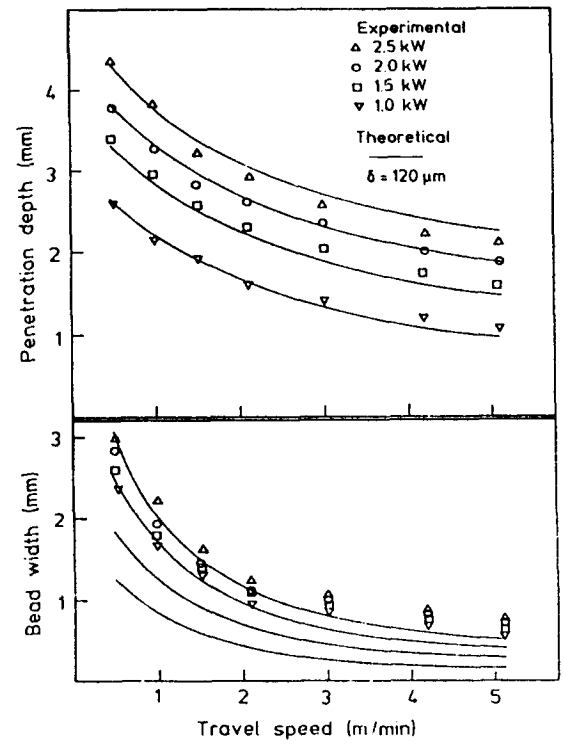

Fig. 8 Comparison of the experimental results with the theoretical model on penetration depth and bead width as a function of travel speed at various laser powers when a focal position is 1.0mm below the material surface in AISI 316 steel

and also gives a reduced weld penetration. At high speed the bead with becomes narrower due to the reduction of the effect of plasma. In fact, the plasma produced during the laser beam welding is more serious in stainless steel than in carbon steel.

As the travel speed decreases at a constant laser power, the extent of the molten metal zone surrounding the keyhole increases in proportional to the increased heat input. Eventually, the metal vapor pressure is insufficient to counter the fluid dynamic forces of the liquid metal and the deep keyhole collapses. Under such a condition an adrupt decrease in penetration occurs at low travel speed (>0.5m/min) and roughly hemispherrical fusion zone is obtained. When the laser employs a very small size of beam, the very deep penetration depth can be predicted even though high travel speed as shown in Fig.9.

Figures 10, 11 show a good agreement between the calculated and observed fusion boundaries based on the beam spot

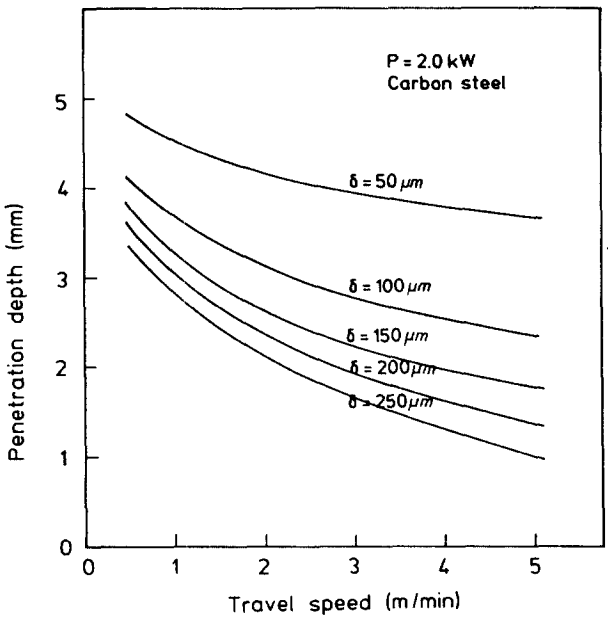

Fig. 9 Calculated penetration depth as a function of travel speed at various beam spot radii at $P=2.0$kW in carbon steel

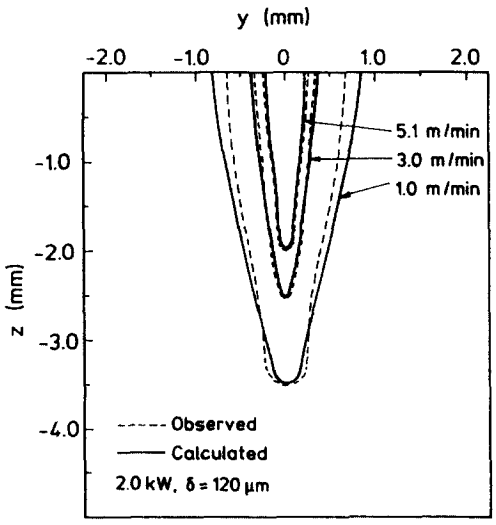

Fig. 10 Comparison between the calculated and observed fusion boundaries of laser welds made at $P=2.0$kW and various travel speeds in carbon steel

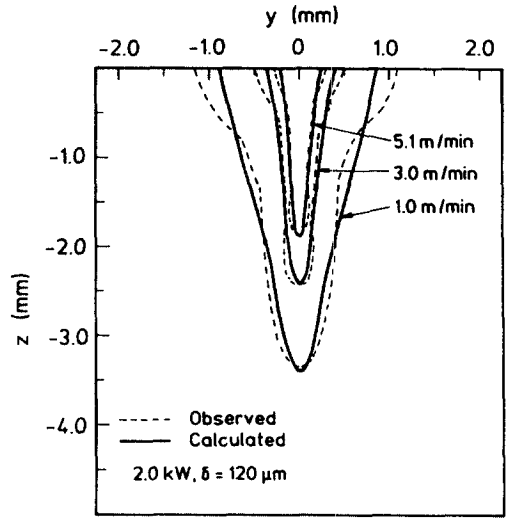

Fig. 11 Comparison between the calculated and observed fusion boundaries of laser welds made at $P=2.0$kW and various travel speeds in AISI 316 steel

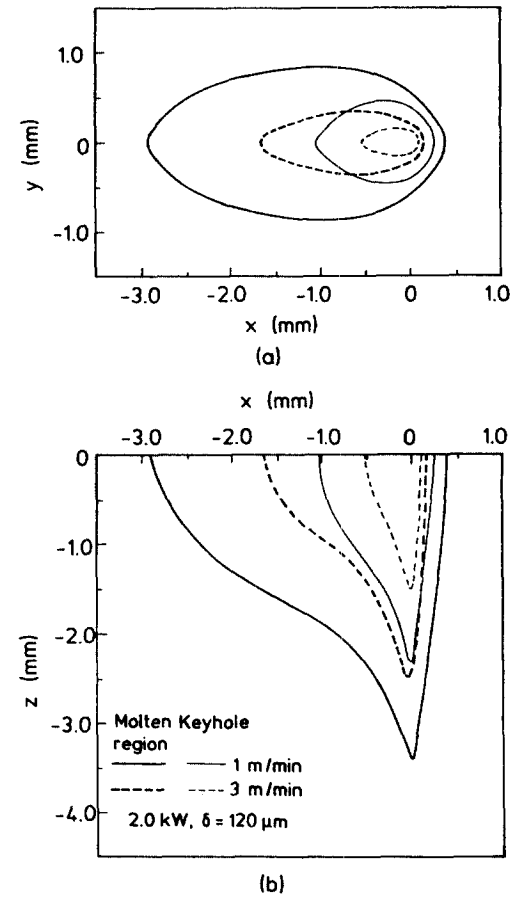

Fig. 12 Calculated boundary contours of fusion and keyhole in carbon steel (a) Top view, (b) Side view

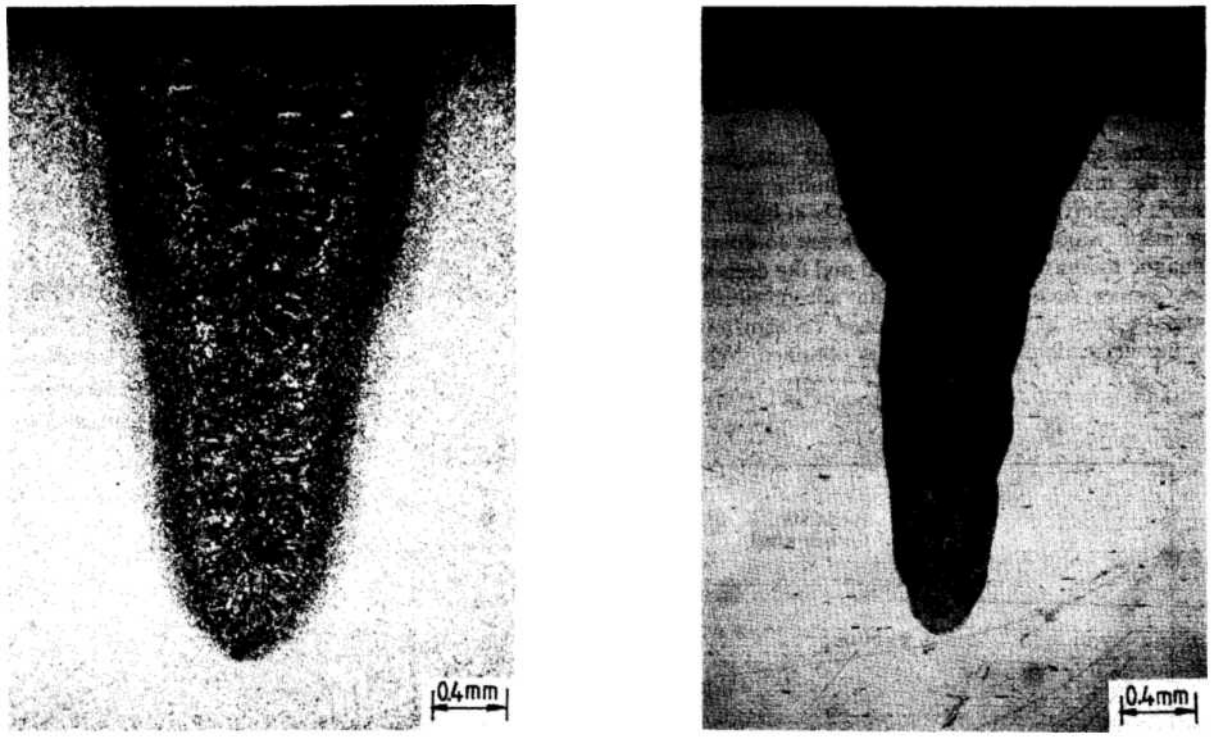

(a) P=2.0kW, v=1.5m/min, carbon steel (b) P=2.0kW, v=1.5m/min, AISI 316 steel

Fig. 13 Macrosections of laser welds

radius of 120μm in carbon and AISI 316 steels. The typical calculated keyholes and fusion boundaries formed around the laser beam are shown in Fig. 12. The keyhole is filled with gas or vapor created bv continuous vaporization of the wall material by the beam. This keyhole is surrounded by molten liquid which in turn is surrounded by solid metal. The narrower weld deposit can be predicted at high travel speed. The cross sections of keyhole and fusion boundary are in a good agreement with the experimental results studied by Arata et al. (1985), using a high speed photography and a trasmission X-ray. Using this approach, the isotherm distributions can be calculated for different laser beam welding conditions.

The microstructure of laser welds in carbon steel shows the full martensite in molton zone. Because of very high cooling rate, there is no time for carbon diffusion and martensite is formed. By comparing the microstructure with the prediction, the cooling rate of the weld area from 800℃ to 500℃ is calculated to be greater 10³℃/sec. This high value is responsible for the full martensite structure in weld area even though a carbon content of carbon steel is fairly low. Figure 13 shows the macrosections of laser welds in carbon steel and AISI 316 steel.

6. CONCLUSIONS

An effective analytical model incoportating a moving Gaussian heat source to predict temperature distribution in the material after beam-metal interaction is detailed. The normalized temperature rise and cooling rate produced by a moving Gaussian beam depends on the ratio of the scanning velocity to the thermal diffusion and on the ratio of the beam spot radius to the absorption depth. In the laser beam welding the maximum possible penetration depth for given sources of laser power, travel speed and beam spot size can be predicted with this model. The calculated penetration depth for carbon and AISI 316 steels are in a good agreement with the experimental results. Also, the calculated bead width and fusion boundary agree reasonably well with the observed ones. High cooling rate is evident due to the nature of the laser beam processing.

REFERENCES

Adams, J.M., 1973, "CO_2 Laser Welding of Aero-Engine Materials", British Welding Institute, Report No. 335/3/73.

Arata, Y. et al., 1985, "Dynamic Observation of Beam Hole during Laser Beam Welding", IIW Doc. IV-396-85.

Breinan, E.M. and Banas, C.M., 1975, "Laser Welding-The Present State of Art", Proc. of SPIE, TelAviv, July, pp. 1~5.

Carslaw, H.C. and Jaeger, J.C., 1959, Condition of Heat in Solids, Clarendon press, London.

Cline, H.E. and Anthony, T.R., 1977, "Heat Treating and Melting Material with a Scanning Laser or Electron Beam", J. of Appl. Phy., Vol. 48, No. 9, pp. 3896~3900.

Davies, M. et al., 1985, "Modeling the Fluid Flow in Laser Beam Welding", Welding. J., Vol. 64, No. 7, pp. 167s~174s.

Hull, D. M. and Stewart, A., 1985, "Laser Beam Profiles, Principles and Definitions", Lasers & Applications, Vol. 10, pp. 75~80.

Keefer, D.R. et al., 1975, "Experimental Study of a Stationary Laser Sustained Air Plasma", J. of Appl. Phy., Vol. 46, No. 3, pp. 1080~1083.

Kim, J.D. and Subramanian, R.V., 1988, "Heat Flow in Laser Beam Welding", 4th Int'l Conf. on Welding by Electron and Laser Beams, Cannes, France, pp. 175~182.

Klemens, P.G., 1976, "Heat Balance and Flow Conductions for Electron Beam and Laser Welding", J. of Appl. Phy., Vol. 47, No.5, pp. 2165~2173.

Maher, W.E. at al., 1974, "Experimental Study of Ignition and Propagation of Laser-supported Detonation Waves", J. of Appl. Phy., Vol. 45, No.5, pp. 2138~2145.

Mazumder, J. and Steen, W.M., 1980, "Heat Transfer Model for CW Laser Material Processing", J. of Appl. Phys., Vol. 51, No.2, pp. 941~947.

Schuöker, D. and Abel, D., 1985, "Material Removal Mechanism of Laser Cutting", Proc. of SPIE, pp. 88~95.

Swift-Hook, D.T. and Gick A.E., 1973, "Penetration Welding with Lasers", Welding J., Vol.52, No. 11, pp. 492s~499s.

Touloukian, Y.S., 1975, Thermophysical Properties of High Temperature Solid Materials, Vol 1-6, The Macmillian Co.

Walker, W., 1984, "Applying Multikilowatt Co_2 Lasers in Industry", Lasers & Applications, Vol. 4, pp. 61~69.